

Notice

This manuscript is a non-peer reviewed preprint submitted to EarthArXiv. It has been submitted for publication to GRL on 01/10/2019 with reference number #2019GL085649. Newer versions may be moderately different with slight variations in content.

Manuscript details

Title: Does a damaged-fault zone mitigate the near-field impact of supershear earthquakes?—Application to the 2018 Mw 7.5 Palu earthquake

Authors: Elif Oral, Huihui Weng and Jean-Paul Ampuero

Contact: elif.oral@geoazur.unice.fr

1 **Does a damaged-fault zone mitigate the near-field**
2 **impact of supershear earthquakes?—Application to the**
3 **2018 M_w 7.5 Palu earthquake**

4 **Elif Oral¹, Huihui Weng¹, and Jean Paul Ampuero^{1,2}**

5 ¹Université Côte d'Azur, IRD, CNRS, Observatoire de la Côte d'Azur, Géoazur, France

6 ²California Institute of Technology, Seismological Laboratory, Pasadena, CA, USA

7 **Key Points:**

- 8 • The unexpectedly low rupture speed of the 2018 Palu supershear earthquake can
9 be explained by a fault damage zone.
- 10 • The reduction of rupture speed by a fault damage zone mitigates the near-field
11 ground motion and landslide hazard.
- 12 • Fault zone waves amplify ground motions, but not enough to compensate for the
13 mitigation effect of rupture speed.

Corresponding author: Elif Oral, elif.oral@geoazur.unice.fr

Abstract

14 **Abstract**
15 The impact of earthquakes can be severely aggravated by cascading secondary hazards.
16 The 2018 M_w 7.5 Palu, Indonesia earthquake led to devastating tsunamis and landslides,
17 while triggered submarine landslides possibly contributed substantially to generate the
18 tsunami. The rupture was supershear over most of its length, but its speed was unex-
19 pectedly low, between the S-wave velocity V_S and Eshelby's speed $\sqrt{2}V_S$, an unstable
20 speed range in conventional theory. Here, we investigate whether dynamic rupture mod-
21 els including a low-velocity fault zone (LVFZ) can reproduce such steady, slow super-
22 shear rupture. We then examine numerically how this peculiar feature of the Palu earth-
23 quake could have affected the near-field ground motion and thus the secondary hazards.
24 Our findings suggest that the presence of a LVFZ can explain the slowness of the rup-
25 ture and may have mitigated the near-field ground motion and induced landslides in Palu.

Plain Language Summary

26 **Plain Language Summary**
27 Earthquakes are produced by slippage quickly unzipping along faults, causing Earth's
28 vibrations that we feel as ground shaking. The shaking can become more catastrophic
29 by triggering other phenomena, like landslides and tsunamis, as did the 2018 Palu (In-
30 donesia) earthquake of magnitude 7.5. Generally, the faster the earthquake rupture, the
31 stronger the shaking. The Palu earthquake is among a class of very fast but rare earth-
32 quakes whose speed exceeds that of shearing waves in rocks. Theoretically these so-called
33 "supershear earthquakes" can propagate steadily only if faster than a speed known as
34 Eshelby's speed; Surprisingly, the Palu earthquake is slower than this limit. How can we
35 explain this slow, steady supershear rupture in Palu? How does it affect the potential
36 of triggering landslides, including submarine landslides that likely contributed to the tsunami.
37 We address these questions through computer simulations, particularly focusing on the
38 possible effect of a "fault damage zone"—softened rocks surrounding faults because of
39 accumulated rock fracturing throughout the past fault activity. We found that, if a dam-
40 age zone exists around the Palu fault, it can explain the slow supershear and may have
41 had the beneficial effect of reducing the shaking, and thus its induced landslide and tsunami
42 hazards in Palu.

43 1 Introduction

44 The 2018 M_w 7.5 earthquake in Palu, Sulawesi, Indonesia, ruptured at a supershear speed. The rupture initiated on an unmapped fault located within the inland Sulawesi neck and propagated 150 km southward on the strike-slip Palu-Koro fault. Studies using teleseismic back-projection revealed that the rupture reached rapidly a steady velocity of about $V_{rup}=4.1$ km/s, exceeding the local S-wave velocity $V_S=3.4-3.8$ km/s (Bao et al., 2019).

50 The rupture speed of the Palu earthquake was unexpectedly low as a supershear earthquake, and here we aim at understanding whether the presence of a damaged-fault zone can be the reason behind it. On the basis of theoretical and experimental studies, a stable rupture propagation at supershear speed is only expected at velocities higher than Eshelby's speed $V_E = \sqrt{2}V_S$ (e.g., Andrews, 1976; Dunham, 2007). Yet, the inferred rupture speed of the Palu event lies in the unstable supershear regime $V_S < V_{rup} < V_E$. One proposed explanation of such a rupture speed is the presence of a low-velocity fault zone (LVFZ). Supershear ruptures in a LVFZ approach the P-wave speed of the LVFZ (Huang et al., 2016). Indeed, Bao et al. (2019) interpreted the observed rupture speed by the possible presence of a LVFZ with 30% velocity reduction. However, previous studies modeling supershear rupture in a LVFZ were based on 2D models that ignored the finiteness of the seismogenic depth, while the Palu earthquake rupture has a high length-to-width ratio (150 km length vs. a typical seismogenic depth of 15-20 km for strike-slip earthquakes). Recent theory and simulations show that the seismogenic width controls the evolution of rupture speed in elongated faults (Weng & Ampuero, 2019). Thus, the first question we address, in section 2, is: can the presence of a LVFZ lead to a slow steady-state supershear rupture (running at the damaged-P-wave speed) in a long rupture with finite seismogenic width?

68 The earthquake also triggered devastating landslides; the rupture properties must have been determinant on the distribution and density of co-seismic landslides. The impact of the earthquake was aggravated by landslides triggered in the proximity of the fault, including submarine landslides in the Palu Bay that likely contributed to the generation of a devastating tsunami (Carvajal et al., 2019). Major co-seismic landslides were reported in four different areas, within 10 km of distance from the fault, on gently-sloping alluvial valley floor (Bradley et al., 2019). Past studies have relied on the empirical eval-

75 uation of earthquake-induced landslide hazard by using seismic factors such as earthquake
 76 magnitude and epicentral distance (e.g., Keefer, 1984; Papadopoulos & Plessa, 2000; Me-
 77 unier et al., 2007). Yet, recent research points to the necessity of considering the com-
 78 bined effect of geo-environmental factors and rupture complexities to improve the haz-
 79 ard prediction. For example, landslides triggered by the 2008 Wenchuan earthquake were
 80 found to be unexpectedly high for a M_w 7.9 event (Xu et al., 2016). Conversely, 1999
 81 M_w 7.2 Düzce and the 2002 M_w 7.9 Denali earthquakes have induced landslides lower
 82 than expected for M7+ earthquakes (Görüm et al., 2011). Indeed, despite the similar-
 83 ities of magnitude, topology, climate and rock type, the difference between the 2015 M_w
 84 7.8 Gorkha and the 2008 Wenchuan earthquake-triggered landslide densities is mainly
 85 associated with the rupture complexities (Xu et al., 2016; Roback et al., 2018). For that
 86 reason, we also investigate the effect of rupture properties of the Palu earthquake on ground
 87 motion and consequent landslide triggering in the near field.

88 We scope to clarify whether the ground motion and the consequent landslide-triggering
 89 impact during the Palu earthquake were mitigated by the lower rupture speed or aggra-
 90 vated by wave amplification due to a damage zone. Among the source properties, rup-
 91 ture speed significantly affects ground motion: a supershear rupture can generate stronger
 92 ground motion than a subshear rupture, except if the rupture propagates at sub-Eshelby
 93 speed (Aagaard & Heaton, 2004; Dunham & Archuleta, 2005; Bizzarri & Spudich, 2008).
 94 On the other hand, waves trapped by a LVFZ can amplify ground motion (Spudich &
 95 Olsen, 2001; Ben-Zion et al., 2003; Peng et al., 2003; Huang et al., 2014; Kurzon et al.,
 96 2014). The Palu earthquake is a sub-Eshelby supershear rupture (relative to the host-
 97 rock wave speed) and may have occurred within a LVFZ: rupture speed and fault zone
 98 structure may have had competing effects on ground motion. Therefore, the second ques-
 99 tion we address, in section 3, is: in the presence of a LVFZ, can a supershear rupture run-
 100 ning at the damaged-P-wave speed aggravate near-field ground motion?

101 **2 Early and sustained supershear at damaged-P-wave speed**

102 **2.1 2.5D dynamic rupture modeling**

103 We model a dynamic rupture on a vertical strike-slip fault with finite seismogenic
 104 width W . For the sake of computational efficiency, we adopt a reduced-dimensionality
 105 (2.5D) model, which has been shown to be a successful approximation of 3D rupture mod-

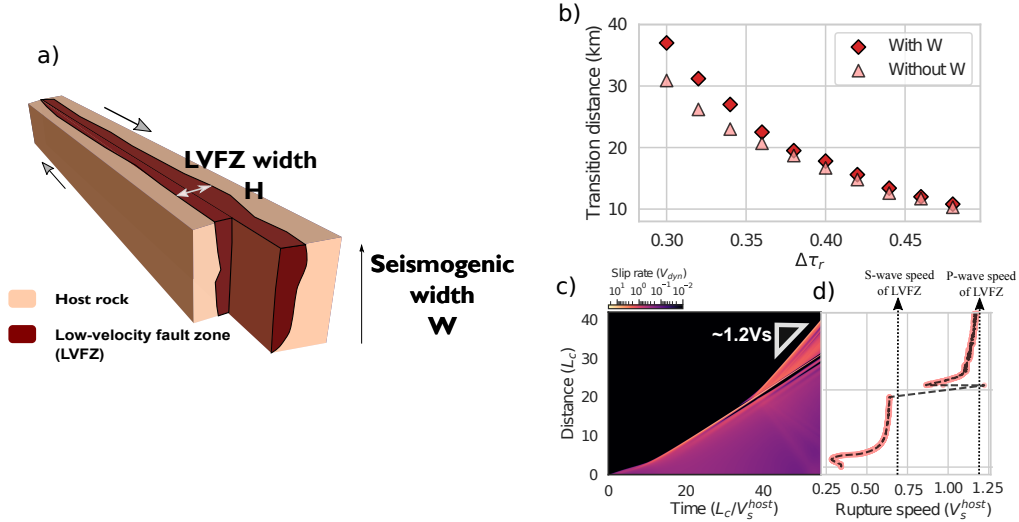


Figure 1. (a) Conceptual model of a low-velocity fault zone. (b) Supershear transition distance as a function of stress drop (normalized by strength drop) in dynamic rupture models with and without finite seismogenic zone. (c) Spatio-temporal distribution of slip rate and (d) rupture speed vs distance along the fault strike for the simulation where $\Delta\tau_r = 0.37$.

106 elms on elongated faults (Weng & Ampuero, 2019). The fault bisects a LVFZ with uni-
 107 form properties, embedded in an unbounded, homogeneous host rock medium (Figure
 108 1a). The LVFZ is defined by its width H and its reduction of P- and S-wave velocities
 109 relative to the host rock, $\Delta V/V$. We set $\Delta V/V = 30\%$, as hypothesized by Bao et al.
 110 (2019). Such a value of velocity reduction is not unusual in mature fault zones (Huang
 111 & Ampuero, 2011). We set a Poisson’s ratio of 0.25 everywhere.

112 We artificially initiate the rupture by prescribing a smooth time-weakening front
 113 that expands at a prescribed speed, $0.25V_s$, as in Andrews (1985). The rupture starts
 114 to propagate spontaneously when the time-weakening front exceeds a critical nucleation
 115 length. Outside the time-weakening zone, the fault is controlled by the linear slip-weakening
 116 friction law (Ida, 1972; Palmer & Rice, 1973), with static and dynamic friction coeffi-
 117 cients $\mu_s = 0.6$ and $\mu_d = 0.1$, respectively, and critical slip distance D_c .

118 We normalize all spatial parameters by the characteristic frictional length $L_c =$
 119 $GD_c/\sigma(\mu_s - \mu_d)$, where G is the shear modulus and σ is the fault normal stress. This
 120 length is proportional to the process-zone size that must be well resolved by the numer-
 121 ical grid (Day et al., 2005). Due to computational constraints, we assume $L_c = 400$ m.

122 Huang et al. (2016) found a correlation between supershear-transition distance, nor-
 123 malized LVFZ width H/L_c and initial background stress. We quantify the initial back-
 124 ground stress by the ratio $\Delta\tau_r$ of stress drop (difference between initial shear stress and
 125 dynamic shear strength $\sigma\mu_d$) to strength drop $\sigma(\mu_s - \mu_d)$. For a given $\Delta\tau_r$, the supershear-
 126 transition distance increases as a function of H/L_c . Here, we set $H = 2L_c$ to mimic
 127 the early superhear transition of the Palu earthquake for a considerably wide range of
 128 initial stress conditions. LVFZ widths most often range between 100 and 400 m, with
 129 some exceptions exceeding 1 km (Huang & Ampuero, 2011). In our model, the LVFZ
 130 width equals 800 m. We set the seismogenic width as $W = 30L_c$, which corresponds
 131 to 12 km.

132 The simulations are done with the spectral element code SEM2DPACK (Ampuero,
 133 2002, 2012). We set the element size sufficiently small to resolve the process-zone size:
 134 $0.1L_c$ and $0.5L_c$ with 9 Gauss-Lobatto-Legendre (GLL) nodes per element edge in the
 135 LVFZ and host-rock media, respectively. Numerical oscillations are mitigated by arti-
 136 ficial damping around the fault. The model domain and the duration of the simulation
 137 are chosen such that the rupture does not reach the fault end, and spurious numerical
 138 reflections at the model boundaries do not reach the rupture. Perfectly Matched Lay-
 139 ers are imposed at all model boundaries.

140 **2.2 Results**

141 Our analyses show that, even when accounting for the finite seismogenic width, the
 142 supershear transition can occur early if the background stress is sufficiently high. We per-
 143 formed simulations at different background stress ratios ranging from 0.2 to 0.48. Fig-
 144 ure 1 (b) shows the supershear-transition distance for each case, compared to the results
 145 without W-effect (2D simulations equivalent to $W = \infty$). The transition occurs at shorter
 146 distances for a higher initial stress. This trend is qualitatively similar to that in the infinite-
 147 W case; the effect of the seismogenic depth slightly delays the supershear transition, by
 148 less than 20%. The calculated transition distance ranges roughly from 4 to 15 km if $\Delta\tau_r$
 149 ranges from 0.3 to 0.5. Considering the uncertainties of relative location in the back-projection
 150 imaging of the Palu earthquake by Bao et al. (2019), these models are consistent with
 151 the observed early supershear-transition distance.

152 The observed rupture speed of the Palu event is not surprisingly low for a dam-
 153 aged fault; the presence of a LVFZ can induce a steady-state supershear rupture at the
 154 damaged-P-wave speed, even on an elongated fault. We further present the rupture prop-
 155 erties in one of the cases where the supershear transition distance is consistent with the
 156 observation, namely the case $\Delta\tau_r = 0.37$. The distribution of slip rate as a function of
 157 distance along strike and time is shown in Figure 1 (c). The rupture is initially sub-shear
 158 and transitions to supershear at a distance of $20 L_c$ (corresponding to 8 km). The rup-
 159 ture speed stabilizes at $\sim 1.2V_s$ (Figure 1d), which is the P-wave speed of the LVFZ medium.
 160 Given the observed rupture speed, 4.1 km/s, for an approximate S-wave speed of host
 161 rock of 3.5 km/s for the Palu event, the results of our dynamic rupture modeling sup-
 162 port the possibility that the LVFZ presence promotes a persistent slow supershear rup-
 163 ture at damaged-P-wave speed.

164 Slow supershear events as the Palu earthquake should not be surprising for major
 165 faults with a pronounced damage zone. Although we focused above on a single set of pa-
 166 rameters that represents well the short supershear-transition distance and slow rupture
 167 features of the Palu event, given that we found the W-effect is not dramatic, the effect
 168 of different values of fault zone width and velocity reduction can be anticipated based
 169 on the findings of comprehensive sensitivity analyses in 2D by Huang and Ampuero (2011);
 170 Huang et al. (2014, 2016). According to these studies, the presence of a LVFZ leads to
 171 a lower critical stress value for supershear transition than in homogeneous media, ow-
 172 ing to dynamic stress perturbations induced by fault zone waves. Moreover, the rupture
 173 speed depends on initial stress and LVFZ properties. If the LVFZ is too narrow (e.g.,
 174 $H < \sim L_c$ if $\Delta V/V = 30\%$) the wavelength of head waves inside the LVFZ is too short
 175 to induce a permanent supershear transition at any initial stress level. If the LVFZ is
 176 too wide ($H > 6L_c$ if $\Delta V/V = 30\%$) very long distances ($> 100L_c$) or high initial
 177 stress values ($\Delta\tau_r > 0.45$) are required to promote supershear speed. Thus, for the case
 178 with 30% velocity reduction, the range of LVFZ widths that likely promotes slow super-
 179 shear rupture is $1 < H/L_c < 6$. This condition implies LVFZ widths ranging from 400
 180 m to 2.4 km for our particular choice of L_c value. Such range involves values near and
 181 above the upper end of real LVFZ widths. A smaller L_c value allows for slow supershear
 182 rupture well within the usual range of natural LVFZ widths. Therefore, rupture prop-
 183 agation at the speed of the Palu earthquake can be expected under a considerably wide
 184 range of conditions, supporting the slow supershear hypothesis of Huang et al. (2016)

185 for past earthquakes such as the 1906 San Francisco and the 1999 M_w 7.1 Düzce earth-
 186 quakes (Ben-Zion et al., 2003; Song et al., 2008). Better constraining LVFZ properties
 187 and L_c could help to test further this hypothesis.

188 **3 Changes in near-field ground motion during a slow supershear rup-** 189 **ture**

190 **3.1 3D wave propagation modeling**

191 To investigate the near-field ground motions during a persistent supershear rup-
 192 ture, we simulated steady-state ruptures in 3D, with prescribed constant stress drop and
 193 constant rupture speed. Following the procedure of Andrews (1985) and Dunham and
 194 Bhat (2008), we force the friction coefficient to weaken linearly as a function of time in-
 195 side a process zone, which propagates at prescribed speed. At the tail of the process zone,
 196 the friction coefficient equals μ_d . To avoid stress singularities at the rupture tip, the peak
 197 fault strength and process zone size are not prescribed but vary spontaneously.

198 We created three different models: Model A is a fast supershear model without LVFZ;
 199 Model B is a slow supershear model with a LVFZ; and Model C is a slow supershear model
 200 without LVFZ. We set $V_S=3.5$ km/s for all models, such that $V_P=6.06$ km/s, $V_E=4.95$
 201 km/s, and Poisson's ratio is 0.25. We set the rupture speed in Model A as 5.95 km/s,
 202 close to the P-wave speed; and in Models B and C as 4.17 km/s, a sub-Eshelby speed.
 203 The element sizes are 0.4 and 1.2 km in the LVFZ and host-rock media, respectively. 5
 204 GLL points are used per spectral element edge. The grid allows for a resolution up to
 205 2 Hz; we apply a Butterworth low-pass filter with 2 Hz corner frequency to all simulated
 206 signals before analysis. The model length, width and depth are 360 km, 180 km and 36
 207 km, respectively. We set the seismogenic width to 12 km. Spurious numerical reflections
 208 from model boundaries are mitigated by absorbing boundary layers. We let the rupture
 209 propagate a distance of 72 km (that is, 6 W). The simulations are conducted with the
 210 SPEC3D software (Kaneko et al., 2008; Tromp et al., 2008; Galvez et al., 2014). We
 211 verified that the final slip is similar in the three models (differences are of about 10 %).

212 We evaluated the induced-landslide potential, in relative terms, by comparing seis-
 213 mic intensity parameters. Many studies of co-seismic landslide susceptibility have used
 214 seismic intensity parameters such as peak ground velocity (PGV), peak ground accel-
 215 eration (PGA) and Arias intensity (I_a). Several quantitative analyses on past co-seismic

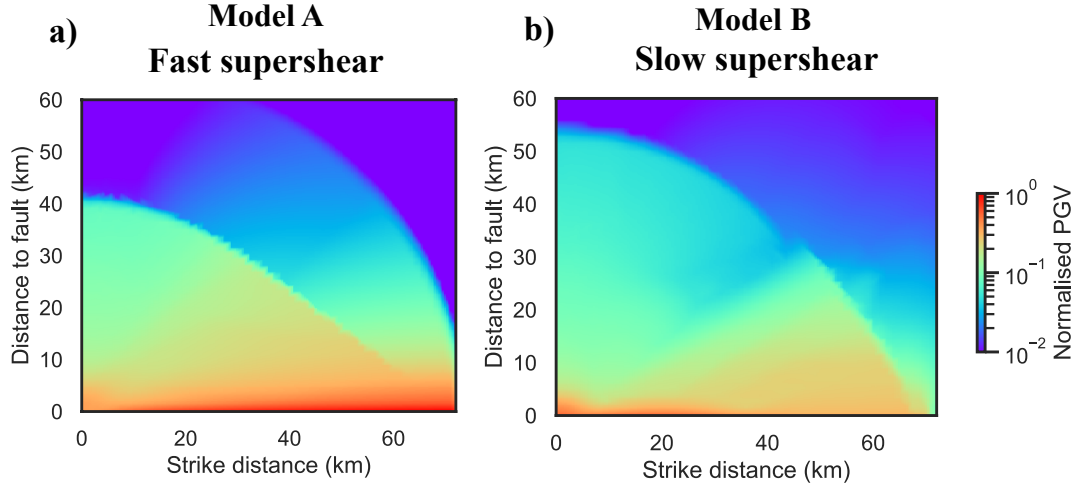


Figure 2. Maximum peak-to-peak amplitude of ground velocities for (a) fast supershear and (b) slow supershear models. All values are normalized by the maximum value of Model A.

216 landslides also point to the correlation between these parameters and observed distri-
 217 bution patterns of landslides (e.g., Refice & Capolongo, 2002; Meunier et al., 2007). Al-
 218 though the combined use of these parameters has been proposed to improve the predic-
 219 tion of landslide displacement (Saygılı & Rathje, 2008), a recent comparative study sug-
 220 gests that all parameters produce similar results (Dreyfus et al., 2013). Therefore, in this
 221 study, we discuss the landslide-triggering impact of ground motion by using PGV. Given
 222 the limitations of our simulations to low frequency (< 2 Hz), we provide PGA and I_a
 223 results only for reference in supplementary material.

224 3.2 Mitigation of near-field landslide hazard by sub-Eshelby rupture speed

225 Peak ground motion is notably attenuated due to the reduction of rupture speed.
 226 As expected, P waves attenuate with distance in both models, and large S-wave ampli-
 227 tudes persist to long distances within Mach cones (Figure 2). The overall spatial exten-
 228 sion of the highest PGV values is wider in Model A than in Model B given the wide ex-
 229 pansion of the Mach cone in Model A due to its high rupture speed.

230 The reduction in ground-motion amplitude is related to the significant attenuation
 231 of waves in the whole frequency band due to the slow supershear speed. We compare the
 232 acceleration spectra between Models A and B at a strike distance of 40 km (Figure S1.1).

233 When the rupture front reaches a distance of 72 km, the Mach cone of Model A has prop-
234 agated to 22 km off the fault at 40 km along strike. Within this distance, the ground mo-
235 tion in Model B is weaker than in Model A at all frequencies (except for the partial am-
236 plification of low-frequency motion of Model B close to the fault in the fault-normal di-
237 rection). This damping effect affects all components of ground motion at the same dis-
238 tance (Figure S1.2).

239 To mimic the landslide-triggering impact of our models on reported landslide lo-
240 cations of the Palu earthquake, we evaluate the ground motion at a fixed along-strike
241 distance. Both submarine and inland landslides of the Palu earthquake are reported at
242 locations that are considerably far from the fault end, and where the rupture presum-
243 ably propagated at a steady state. In addition, these sites are located at comparable dis-
244 tances in units of W , such that we interpret the landslide hazard of these sites by an-
245 alyzing the ground motion at different off-fault distances but at a fixed along-strike dis-
246 tance.

247 The analyses on peak-ground velocities point to the reduction of landslide-triggering
248 potential in the slow supershear model. We compare the dependence of PGV on off-fault
249 distance at a strike distance of 40 km—we verified that the rupture reached steady state
250 there—between Models A and B (Figure 3a). The largest values occur in the vicinity
251 of the fault in both models, and the difference of PGV between the models vanishes with
252 increasing distance to the fault. Within the distance of Mach-front propagation (< 22
253 km), the PGV values of the fast supershear model are higher than those of the slow su-
254 pershear model.

255 Our results support the findings of past studies: a smaller rupture speed (here caused
256 by the presence of a LVFZ) results in a significant reduction of the amplitudes of near-
257 field ground motion and consequent landslide-triggering impact, and this influence of rup-
258 ture speed on ground motion is valid at various distances from the fault (within 30 km
259 here).

260 **3.3 Enhanced high-frequency ground motion and landslide hazard caused** 261 **by damage**

262 High-frequency waves are amplified due to the damaged-fault zone over a wide range
263 of off-fault distances. To isolate the effect of the presence of a LVFZ, we compare two

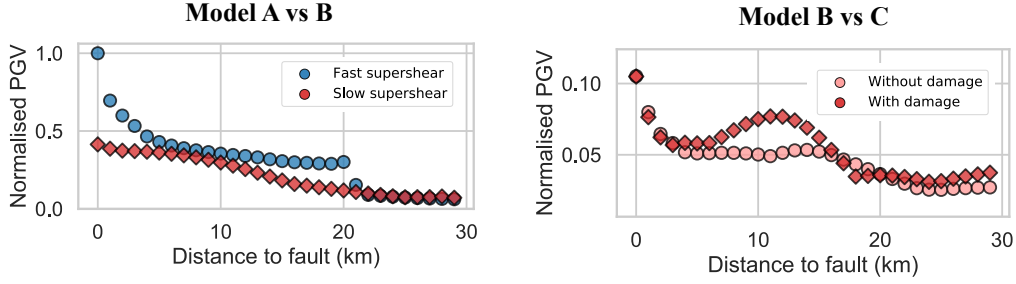


Figure 3. Comparison of peak ground velocities vs distance from the fault between fast (Model A) and slow (Model B) supershear models (a), and between slow supershear models with damage (Model B) and without damage (Model C) (b). All values are normalized by the maximum value of the Model A.

264 slow supershear models with and without LVFZ (Models B and C, respectively). Our
 265 analysis of acceleration spectra suggests that the presence of a LVFZ results in slight am-
 266 plification of the ground motion, in particular at frequencies above 0.5 Hz (Figure S1.4).
 267 This is expected, since the resonance frequency of waves normally reflected at the LVFZ-
 268 host rock interface is 0.39 Hz.

269 The high-frequency amplification due to the damaged-fault zone leads to the in-
 270 crease of landslide-triggering impact based on our analyses. We compare the PGV val-
 271 ues of the two models in Figure 3 (b). In both, PGV decays with off-fault distance; but
 272 in the presence of a LVFZ (model B), the PGV values are amplified because of enhanced
 273 high-frequency radiation. To well constrain the effect of the LVFZ, we made the com-
 274 parison in the frequency band of 0.5-2 Hz; PGV amplification due to the LVFZ at a strike
 275 distance of 40 km is pronounced particularly between approximately 6 and 16 km.

276 The reflections due to the velocity contrast between the LVFZ and host rock can
 277 result in an amplified high-frequency motion that could also increase the landslide-triggering
 278 impact at farther distances to the fault. Considering the extent of the sites where land-
 279 slides are reported, our results indicate that the landslide triggering potential of the Palu
 280 earthquake may have been aggravated by the presence of a damaged-fault zone (com-
 281 parison of Model B and C). Yet, in the previous subsection, we found a dampening ef-
 282 fect of the LVFZ on landslide triggering potential, via its effect on rupture velocity (com-

283 parison of Model A and B). Out of these two competing effects of the LVFZ, the former
284 one (amplification) is relatively slight.

285 **4 Conclusions and Discussion**

286 Our 2.5D dynamic rupture models of the Palu earthquake suggest that, also for elongated-
287 fault ruptures that saturate the seismogenic thickness, the presence of a damaged-fault
288 zone can promote an early and persistent supershear rupture at a speed that is unex-
289 pectedly slow for intact rock, namely the P-wave speed of the damaged rock.

290 The near-field ground motion produced by a supershear rupture is much weaker
291 if it runs at the damaged-P-wave speed and if this speed is lower than the Eshelby's speed
292 of the host rock. The presence of a damaged-fault zone also amplifies high-frequency ground
293 motion (> 0.5 Hz) up to long distances from the fault (30 km). Yet, the latter effect is
294 weaker, thus overall the presence of a LVFZ mitigates the near-field ground motion and
295 its landslide triggering potential.

296 Our findings support the strong influence of the rupture dynamics and fault zone
297 structure on near-field ground motion and earthquake-induced landslides. The results
298 of our simplified modeling can serve as a reference for more realistic studies where to-
299 pography, heterogeneous material properties, and liquefaction potential are accounted
300 for on a broader frequency band.

301 Our results can be helpful for further understanding the role of low-velocity fault
302 zones on past and future earthquakes (e.g., Perrin et al., 2016). For example, the pres-
303 ence of a damaged-fault zone was speculated as an explanation of the difference of rup-
304 ture speed between the northern and southern sides of the fault during the 1999 M_w 7.4
305 İzmit earthquake (Bouchon et al., 2001). Mai (2019) draws attention to the striking sim-
306 ilarities between the İzmit and Palu cases for further earthquake mitigation programs—
307 the rupture of İzmit earthquake also propagated for 150 km on a strike-slip fault; and
308 co-seismic tsunamis were triggered and locally amplified presumably because of tectonic
309 subsidence and submarine landslides within the narrow İzmit Bay (Yalçınler et al., 2000).

310 **Acknowledgments**

311 This work was supported by the French National Research Agency (ANR) through project
312 FAULTS_R_GEMS (grant ANR-17-CE31-0008) and Investments-in-the-Future project

UCAJEDI (grant ANR-15-IDEX-01). We acknowledge Luis A. Dalguer for helpful comments that improved the content of this manuscript. All data to reproduce this work is available online: 2D and 3D wave propagation modeling tools can be found at <https://github.com/jpampuero/sem2dpack> and <https://github.com/geodynamics/specfem3d> addresses.

References

- Aagaard, B. T., & Heaton, T. H. (2004). Near-source ground motions from simulations of sustained intersonic and supersonic fault ruptures. *Bulletin of the Seismological Society of America*, *94*(6), 2064–2078.
- Ampuero, J.-P. (2002). Etude physique et numérique de la nucléation des séismes. *PhD Thesis, University of Paris VII, France*.
- Ampuero, J.-P. (2012). A spectral element method tool for 2d wave propagation and earthquake source dynamics users guide.
- Andrews, D. (1976). Rupture velocity of plane strain shear cracks. *Journal of Geophysical Research*, *81*(32), 5679–5687.
- Andrews, D. (1985). Dynamic plane-strain shear rupture with a slip-weakening friction law calculated by a boundary integral method. *Bulletin of the Seismological Society of America*, *75*(1), 1–21.
- Bao, H., Ampuero, J.-P., Meng, L., Fielding, E. J., Liang, C., Milliner, C. W., . . . Huang, H. (2019). Early and persistent supershear rupture of the 2018 magnitude 7.5 palu earthquake. *Nature Geoscience*, *12*(3), 200–205.
- Ben-Zion, Y., Peng, Z., Okaya, D., Seeber, L., Armbruster, J. G., Ozer, N., . . . Aktar, M. (2003). A shallow fault-zone structure illuminated by trapped waves in the karadere–düzce branch of the north anatolian fault, western turkey. *Geophysical Journal International*, *152*(3), 699–717.
- Bizzarri, A., & Spudich, P. (2008). Effects of supershear rupture speed on the high-frequency content of s waves investigated using spontaneous dynamic rupture models and isochrone theory. *Journal of Geophysical Research: Solid Earth*, *113*(B5).
- Bouchon, M., Bouin, M.-P., Karabulut, H., Toksöz, M. N., Dietrich, M., & Rosakis, A. J. (2001). How fast is rupture during an earthquake? new insights from the 1999 turkey earthquakes. *Geophysical Research Letters*, *28*(14), 2723–2726.

- 345 Bradley, K., Mallick, R., Alfian, D., Andikagumi, H., Benazir, B., Brocard, G., ...
346 others (2019). Wet rice cultivation was the primary cause of the earthquake-
347 triggered palu landslides.
- 348 Carvajal, M., Araya-Cornejo, C., Sepúlveda, I., Melnick, D., & Haase, J. S. (2019).
349 Nearly instantaneous tsunamis following the mw 7.5 2018 palu earthquake.
350 *Geophysical Research Letters*, *46*(10), 5117–5126.
- 351 Day, S. M., Dalguer, L. A., Lapusta, N., & Liu, Y. (2005). Comparison of finite
352 difference and boundary integral solutions to three-dimensional spontaneous
353 rupture. *Journal of Geophysical Research: Solid Earth*, *110*(B12).
- 354 Dreyfus, D., Rathje, E. M., & Jibson, R. W. (2013). The influence of different sim-
355 plified sliding-block models and input parameters on regional predictions of
356 seismic landslides triggered by the northridge earthquake. *Engineering geology*,
357 *163*, 41–54.
- 358 Dunham, E. M. (2007). Conditions governing the occurrence of supershear ruptures
359 under slip-weakening friction. *Journal of Geophysical Research: Solid Earth*,
360 *112*(B7).
- 361 Dunham, E. M., & Archuleta, R. J. (2005). Near-source ground motion from steady
362 state dynamic rupture pulses. *Geophysical Research Letters*, *32*(3).
- 363 Dunham, E. M., & Bhat, H. S. (2008). Attenuation of radiated ground motion
364 and stresses from three-dimensional supershear ruptures. *Journal of Geophysi-
365 cal Research: Solid Earth*, *113*(B8).
- 366 Galvez, P., Ampuero, J.-P., Dalguer, L. A., Somala, S. N., & Nissen-Meyer, T.
367 (2014). Dynamic earthquake rupture modelled with an unstructured 3-d spec-
368 tral element method applied to the 2011 m 9 tohoku earthquake. *Geophysical
369 Journal International*, *198*(2), 1222–1240.
- 370 Görüm, T., Fan, X., van Westen, C. J., Huang, R. Q., Xu, Q., Tang, C., & Wang, G.
371 (2011). Distribution pattern of earthquake-induced landslides triggered by the
372 12 may 2008 wenchuan earthquake. *Geomorphology*, *133*(3-4), 152–167.
- 373 Huang, Y., & Ampuero, J.-P. (2011). Pulse-like ruptures induced by low-velocity
374 fault zones. *Journal of Geophysical Research: Solid Earth*, *116*(B12).
- 375 Huang, Y., Ampuero, J.-P., & Helmberger, D. V. (2014). Earthquake ruptures
376 modulated by waves in damaged fault zones. *Journal of Geophysical Research:
377 Solid Earth*, *119*(4), 3133–3154.

- 378 Huang, Y., Ampuero, J.-P., & Helmberger, D. V. (2016). The potential for super-
379 shear earthquakes in damaged fault zones—theory and observations. *Earth and*
380 *Planetary Science Letters*, *433*, 109–115.
- 381 Ida, Y. (1972). Cohesive force across the tip of a longitudinal-shear crack and grif-
382 fith’s specific surface energy. *Journal of Geophysical Research*, *77*(20), 3796–
383 3805.
- 384 Kaneko, Y., Lapusta, N., & Ampuero, J.-P. (2008). Spectral element modeling of
385 spontaneous earthquake rupture on rate and state faults: Effect of velocity-
386 strengthening friction at shallow depths. *Journal of Geophysical Research:*
387 *Solid Earth*, *113*(B9).
- 388 Keefer, D. K. (1984). Landslides caused by earthquakes. *Geological Society of Amer-*
389 *ica Bulletin*, *95*(4), 406–421.
- 390 Kurzon, I., Vernon, F. L., Ben-Zion, Y., & Atkinson, G. (2014). Ground motion
391 prediction equations in the san jacinto fault zone: Significant effects of rup-
392 ture directivity and fault zone amplification. *Pure and Applied Geophysics*,
393 *171*(11), 3045–3081.
- 394 Mai, P. M. (2019). Supershear tsunami disaster. *Nature Geoscience*, *12*(3), 150.
- 395 Meunier, P., Hovius, N., & Haines, A. J. (2007). Regional patterns of earthquake-
396 triggered landslides and their relation to ground motion. *Geophysical Research*
397 *Letters*, *34*(20).
- 398 Palmer, A. C., & Rice, J. R. (1973). The growth of slip surfaces in the progres-
399 sive failure of over-consolidated clay. *Proceedings of the Royal Society of Lon-*
400 *don. A. Mathematical and Physical Sciences*, *332*(1591), 527–548.
- 401 Papadopoulos, G. A., & Plessa, A. (2000). Magnitude–distance relations for
402 earthquake-induced landslides in greece. *Engineering Geology*, *58*(3-4), 377–
403 386.
- 404 Peng, Z., Ben-Zion, Y., Michael, A. J., & Zhu, L. (2003). Quantitative analysis of
405 seismic fault zone waves in the rupture zone of the 1992 landers, california,
406 earthquake: evidence for a shallow trapping structure. *Geophysical Journal*
407 *International*, *155*(3), 1021–1041.
- 408 Perrin, C., Manighetti, I., Ampuero, J.-P., Cappa, F., & Gaudemer, Y. (2016). Lo-
409 cation of largest earthquake slip and fast rupture controlled by along-strike
410 change in fault structural maturity due to fault growth. *Journal of Geophysical*

- 411 *Research: Solid Earth*, 121(5), 3666–3685.
- 412 Refice, A., & Capolongo, D. (2002). Probabilistic modeling of uncertainties in
413 earthquake-induced landslide hazard assessment. *Computers & Geosciences*,
414 28(6), 735–749.
- 415 Roback, K., Clark, M. K., West, A. J., Zekkos, D., Li, G., Gallen, S. F., . . . Godt,
416 J. W. (2018). The size, distribution, and mobility of landslides caused by the
417 2015 mw7. 8 gorkha earthquake, nepal. *Geomorphology*, 301, 121–138.
- 418 Saygili, G., & Rathje, E. M. (2008). Empirical predictive models for earthquake-
419 induced sliding displacements of slopes. *Journal of Geotechnical and Geoenvi-*
420 *ronmental Engineering*, 134(6), 790–803.
- 421 Song, S. G., Beroza, G. C., & Segall, P. (2008). A unified source model for the
422 1906 san francisco earthquake. *Bulletin of the Seismological Society of Amer-*
423 *ica*, 98(2), 823–831.
- 424 Spudich, P., & Olsen, K. (2001). Fault zone amplified waves as a possible seismic
425 hazard along the calaveras fault in central california. *Geophysical Research Let-*
426 *ters*, 28(13), 2533–2536.
- 427 Tromp, J., Komatitsch, D., & Liu, Q. (2008). Spectral-element and adjoint methods
428 in seismology. *Communications in Computational Physics*, 3(1), 1–32.
- 429 Weng, H., & Ampuero, J.-P. (2019). The dynamics of elongated earthquake rup-
430 tures. *Journal of Geophysical Research: Solid Earth*.
- 431 Xu, C., Xu, X., Tian, Y., Shen, L., Yao, Q., Huang, X., . . . Ma, S. (2016). Two
432 comparable earthquakes produced greatly different coseismic landslides: The
433 2015 gorkha, nepal and 2008 wenchuan, china events. *Journal of Earth Sci-*
434 *ence*, 27(6), 1008–1015.
- 435 Yalçımer, A. C., Altınok, Y., Synolakis, C. E., Borrero, J., Imamura, F., Ersoy, S., . . .
436 others (2000). Tsunami waves in izmit bay. *Earthquake Spectra*, 16(SUPPL.
437 A), 55–62.